50th AIAA/ASME/ASCE/AHS/ASC Structures, Structural Dynamics, and Materials Conference
17th
4 - 7 May 2009, Palm Springs, California

AIAA 2009-2545

Multiscale Model for Progressive Damage and Failure of Laminated Composites Using an Explicit Finite Element Method

Evan J. Pineda* and Anthony M. Waas†
University of Michigan, Ann Arbor, MI 48109

Brett A. Bednarcyk‡
NASA Glenn Research Center, Cleveland, OH 44135

Craig S. Collier §
Collier Research Corporation, Newport News, VA 23607

Initial development of a multiscale progressive damage and failure analysis tool for laminated composite structures is presented. The method models microdamage at the lamina level with the thermodynamically based Schapery Theory. Transverse cracking and fiber breakage, considered failure mechanisms in this work, are modeled with failure criteria evaluate at the micro-constituent level using the Generalized Method of Cells. This model is implemented using ABAQUS/Explicit finite element software and MAC/GMC Suite of Micromechanics Codes. Load versus displacement and local strain gage results for two center-notched laminates are compared against results using ABAQUS/Standard and experimental data. Furthermore, damage and failure paths are compared to C-scans and photographs of failed specimens.

I. Introduction

ANALYSIS of fiber reinforced laminates (FRLs) remains an ongoing and continuously developing research topic. Numerous theoretical and computational models exist that investigate, describe, and predict the non-linear behavior of damaging FRLs. Supplementing these studies are experimental programs that provide insight into the underlying physics responsible for the observed damage and failure mechanisms in FRLs. A common objective among these various avenues of research are to develop predictive tools capable of accurately quantifying the response of structures composed of FRLs; thus, reducing the volume of tests necessary to validate structural. These tools, implemented computationally, provide designers with tremendous flexibility, allowing a large number of designs to be evaluated, relatively quickly. Accurate, robust models result in trustworthy designs; therefore, only the best designs require physical testing. This ultimately leads to optimally designed, more durable, inexpensive, and safer composite structures.

One of the keys to predicting the overall behavior of composite structures is accurately modeling the complex damage and failure mechanisms that arise in the material. What complicates analyses is that FRL materials are hierarchichal, consisting of several length scales, starting at the fiber and matrix constituent scale, and progressing upwards through inter-laminar interfaces to arrive at the structural FRL scale. The damage mechanisms that develop in the constituents include microcracking, shear banding, and transverse cracking in the matrix, fiber-matrix debonding at the fiber-matrix interface, breakage, pull-out and kinking in the fiber, and delamination in the layer interfaces.[1] The constituents in the material behave just as components in larger scale structures, and the globally observed damage modes result from the responses of the individual constituents and and also through their interactions, including failure mechanisms that can interact.[2] For instance, fiber kinking and pull-out is heavily dependent on the properties of the matrix; whereas, transverse matrix cracks are impeded by the presence of fibers. Additionally, the length scales of the different mechanisms vary. The order in which the damage mechanisms accrue cannot be assumed a priori and may change with structural design and loading scenario. Furthermore, large stress and strain gradients near cut-outs, which are present in most practical applications, further influence the damage and failure evolution.[3,4] In order to accurately *predict* the response of composite materials subjected to loads, these details should be accounted for, and mechanism

*Ph.D Candidate, Mechanical Engineering Department.
†Professor, Aerospace and Mechanical Engineering Departments.
‡Materials Research Engineer, AIAA Senior Member.
§President, Hypersizer Software, AIAA Senior Member

based models must be in place. However, for the models to be used practically, they must require a minimal amount of user inputs and be computationally feasible.

Additionally, a distinction between damage and failure must be established. Progressive damage manifests as a diffusely distributed phenomenon that results in the gradual degradation in the stiffness of a material. A damaged region may still sustain significant loads. Failure, however, is localized and results in the complete reduction of stiffness at the failed region. Local failure may be the truncation of damage or may develop from flaws not associated with damage evolution; after which, the material loses all load carrying capability in the failed area. The various mechanisms responsible for non-linear behavior and stiffness degradation in FRLs can arise as progressive damage and/or failure.

Currently, numerous approaches for modeling damage and failure in composites exist. These theories are often grouped into the category progressive failure analysis (PFA). A comprehensive review of current achievements in PFA is presented by Tay et. al.,[5] and in the recent book by Tsai[6] containing an excellent collection of papers, exercises and tutorials on the subject. Some methods included in PFA for predicting damage and failure in composites are: failure theories,[7–14] continuum damage mechanics,[15–27] and fracture mechanics.[28–37] Micromechanics can also be used to analyze damage and failure in composites.[38–44] Moreover, as available computational power continues to grow, the push towards multiscale methods increases.[45–52]

This paper presents initial work towards the development of a three-level, physics-based, multiscale progressive damage and failure analysis tool. At the structural level, design optimization and sizing iterations will occur using the commercially available Hypersizer Structural Sizing Software.[53] Hypersizer will provide loading conditions for the various components in the structure, and theses components will be analyzed using finite element analysis (FEA) with ABAQUS Finite Element Software[54] at the lamina/laminate level. Lamina-level damage or failure theories can be employed at this stage to model the component. At each material point in the finite element (FE) model, the analysis scale can be further refined to the micro-level where the MAC/GMC Suite of Micromechanics Codes[55,56] performs micromechanical analyses. Information from all three levels is shared to refine the inputs for each level. A schematic of this three level architecture is shown in Figure 1.

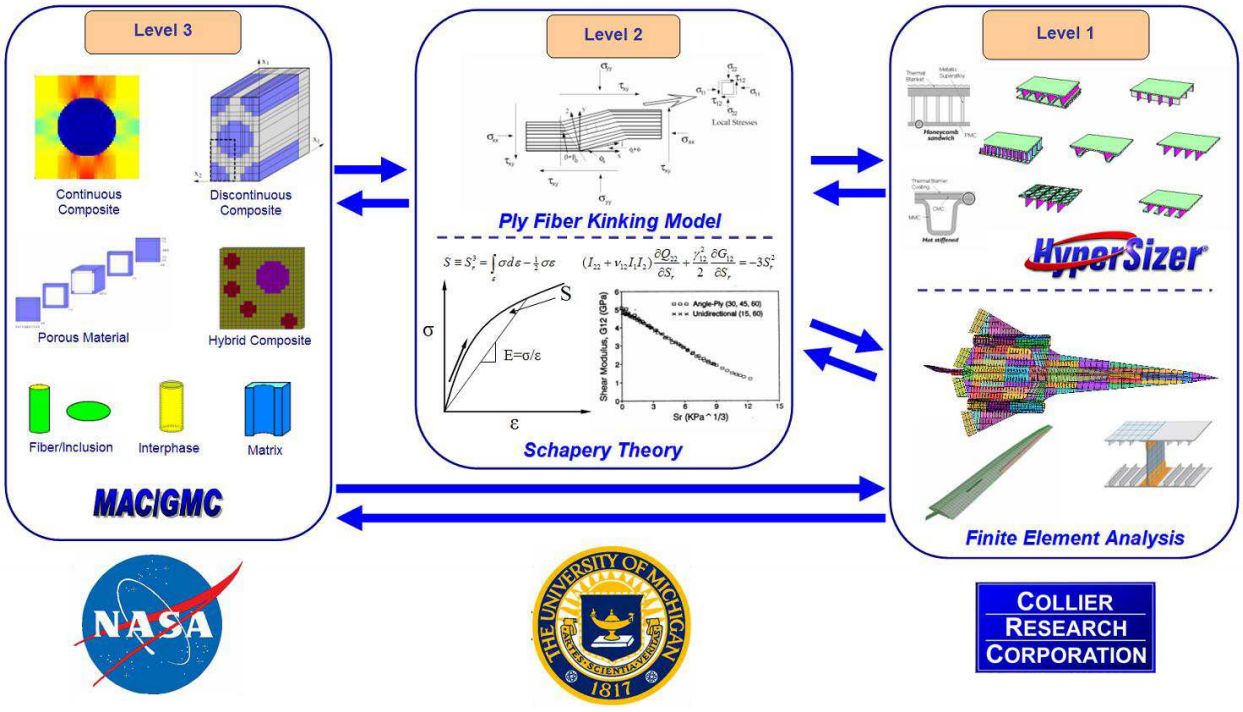

Figure 1. Hierarchy of three-level, multiscale, progressive damage and failure analysis tool for advanced composite structures.

The focus of the current paper is on the lamina/laminate and mirco-scales. Progressive matrix microdamage, which includes microcracking, shear banding, fiber microbuckling, fiber/matrix debonding, and fissure growth, is determined at the lamina level using the thermodynamically based Schapery Theory (ST).[17] ST calculates the amount of energy available to produce the structural changes associated with microdamage and the relation of the composite moduli to that energy. Although ST can also account for transverse cracking through the addition of another internal

state variable (ISV),[18,57] this preliminary work uses micromechanics to model transverse cracks. The Generalized Method of Cells (GMC) developed by Paley and Aboudi[58] divides a repeating volume element (RVE) into a number of constituent subcells. The applied strains or stresses are resolved into local subcell stresses and strains. The method provides the local subcell information in semi-closed form; therefore, it is ultra-efficient and ideal for multiscale analysis. In this work, the truncation of microdamage and the transition to transverse cracking is modeled as a failure mechanism with failure criteria evaluated at the subcell level. This transition occurs abruptly, once the failure criterion is satisfied; however, since the failure is occurring within the subcells, the lamina-level effects of the microscale failure are somewhat progressive. The authors advocate the use of more realistic theories to capture the growth and effects of transverse cracks because failure criteria do not capture any of the physics of transverse cracking and are extremely mesh dependent. However, in this preliminary work, the objective is to effectively capture matrix microdamage, and mark the termination of microdamage with failure dictated by information from the microscale. Fiber failure is also determined using a failure criterion evaluated at the micro-level. A mechanism based failure theory can be used to dictate the fiber failure response but this has not been incorporated in this initial development.

Previous studies[51,52,59] reported the results of analysis using an implicit finite element method (FEM). Unfortunately, the large and abrupt changes in local material properties arising from material softening due to damage and material failure can cause significant convergence issues since local unstable equilibrium paths require a solver that accomodates a *local* snap back in the response. That is, in an incremental solution process, when the material is locally unstable (but, globally stable), the subsequent increment requires a reduction in *both* local strain and stress. A special solution procedure is required to enforce this requirement. In a laboratory setting, this instability signals the onset of a catastrophic failure, leading to large changes in the local stiffness of the material. Such an event can be captured with the use of an explicit solver for the FEM calculations. Using an explicit solver places no restrictions on the degradation of material properties and provides accurate results assuming that a sufficiently small time step is used. Results from the model using ABAQUS/Explicit to analyze two center-notched laminates are compared to model results using ABAQUS/Standard and experimental data[60] in Section V.

II. Lamina Level Modeling of Progressive Microdamage Using Schapery Theory

II.A. Thermodynamically based work potential model

Progressive damage in composites is modeled using ST.[17] This thermodynamics based, work potential theory is capable of capturing the effects of microdamage mechanisms responsible for material nonlinearity by separating the total applied work potential, W_T, into a recoverable part (elastic), W, and a dissipated portion (free energy available to generate structural changes in the material), W_S.

$$W_T = W + W_S \tag{1}$$

As the material is loaded, a portion of the applied work potential facilitates structural changes in the material. These structural changes, such as microcracking, affect the elastic properties of the material. Some of the total applied work potential is recovered when the structure is unloaded. The magnitude of energy recovered is contingent upon the current, degraded elastic properties. Upon subsequent reloading, the material behaves linearly exhibiting the elastic properties observed during unloading, until the material reaches the previous maximum strain state. After this state is achieved, structural changes resume further degrading the elastic moduli of the material. This process is shown in Figure 2. The area labeled "S" represents W_S, and the shaded area under the linear unloading curve is W. It is assumed that the material behaves as a secant material, a reasonable assumption for FRLs.[18]

Both W and W_S are functions of a set of ISVs, S_m, $(m = 1, 2, M)$. These ISVs account for any inelastic structural changes in the material. Differentiating W_S with respect to a general ISV, S_m yields the thermodynamic force, f_m, available for producing structural changes associated with the m^{th} ISV.

$$f_m = \frac{\partial W_s}{\partial S_m} \tag{2}$$

It is shown in Ref. 17 that the total work potential is stationary with respect to each ISV.

$$\frac{\partial W_T}{\partial S_m} = 0 \tag{3}$$

Additionally, Rice[61] shows that according to the second law of thermodynamics:

$$f_m \dot{S}_m \geq 0 \tag{4}$$

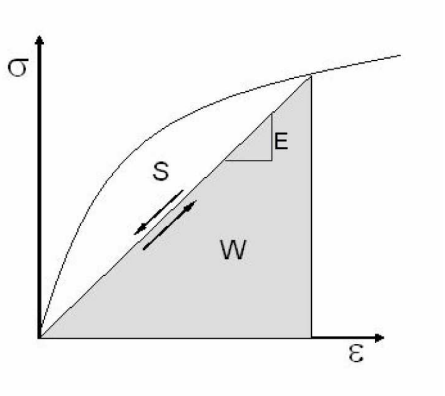

Figure 2. Typical stress-strain curve showing the elastic (W) and irrecoverable (S) portions.

Equations (2), (3), and (4) form the foundation of a thermodynamically based work potential model for nonlinear structural changes in a damaging material.

II.B. Application of ST to model progressive microdamage in fiber reinforced plastic composites: the lamina scale

Damage accumulates in a composite through numerous mechanisms affecting the constituent materials in the composite. Micro-level damage, which includes matrix microcracking, micro-void growth, shear banding, fiber/matrix debonding and fiber kinking, is a class of damage mechanisms separate from matrix failure due to transverse cracking. Matrix microdamage accumulates gradually at the micro-level until its effects are superseded by the progression of transverse cracks, or other larger-scale mechanisms. A larger crack may be a product of the accumulation of many microcracks in a highly damaged region, or it may result from an individual flaw, not necessarily in a microdamaged area, reaching a critical state. Additionally, fiber damage does not typically occur progressively, but rather, abruptly. Moreover, once the fibers in a composite lamina begin to break, it has nearly lost its entire load carrying capabilities. Across the breakline, however, the adjacent layers carry the loads through load re-distribution. Unfortunately, microdamage mechanisms are often overlooked in analyses. ST is capable of modeling the effects of progressive microdamage in the matrix phase of FRLs.

The inelastic free energy available to advance structural changes, W_S, can be a function of any number of state variables. It is assumed that the structural changes which result from microdamage, depend on only one ISV, S. This ISV is assumed responsible for all material nonlinearities up to transverse matrix cracking, delamination and fiber breakage. It should be noted, that additional ISVs may be included to account for additional damage and failure mechanisms. Schapery and Sicking use a two ISV formulation to capture both microdamage and transverse cracking in Ref. 57.

It can be assumed that W_S is an additive function of the ISVs, $W_S = \sum_i^m W_i(S_i)$. Furthermore, W_i are in one-to-one correspondence with their arguments; so, W_i can be chosen such that $W_i = S_i$. Since, in this case, W_S is a function of only one ISV, $W_S = S$. Therefore, the ISV governing the amount of energy used to advance microdamage and that actual energy are equivalent. Equation (1) can now be recast.

$$W_T = W + S \tag{5}$$

Differentiating (5) with respect to S, and utilizing Equation (3) yields:

$$\frac{\partial W}{\partial S} = -1 \tag{6}$$

Additionally, combining Equations (2) and (4) with $W_S = S$ results in

$$\dot{S} \geq 0 \tag{7}$$

which is a statement on the inadmissibility of damage "healing". Equation (7) dictates that the amount of energy used to progress microdamage can never decrease; therefore, that energy has been dissipated into advancing structural change and cannot be recovered. The combination of Equations (6) and (7) represent the evolution equations for microdamage in the matrix of the composite.

II.C. Determining the damage state

It is necessary to define the manner in which the moduli degrade as functions of the ISV. Since the damage mechanisms associated with S accrue only in the matrix of the composite, it is safe to assume that the moduli affected by this damage are limited to the transverse (E_{22}) and shear stiffness, (G_{12}). These moduli can be written as functions of S

$$E_{22} = E_{220} e_s(S) \tag{8}$$

$$G_{12} = G_{120} g_s(S) \tag{9}$$

where E_{220} and G_{120} are the undamaged transverse and shear elastic moduli, $e_s(S)$ and $g_s(S)$ are factors relating the transverse and shear moduli to the microdamage, S. Sicking[18] provides a procedure for determining e_s and g_s experimentally. The experimental curves can then be fit with polynomials (such that when $S = 0$, $E_{22} = E_{220}$ and $G_{12} = G_{120}$) and used in Equations (8) and (9).

For a FRL plate, the elastic strain energy density W can be written using plane stress constitutive relationships, assuming $\nu_{12}\nu_{21} \ll 1$.

$$W = \frac{1}{2}(E_{11}\epsilon_{11}^2 + E_{22}\epsilon_{22}^2 + G_{12}\gamma_{12}^2) + Q_{12}\epsilon_{11}\epsilon_{22} \tag{10}$$

Employing Equation (6) with (8), (9), and (10), and assuming the quantity $Q_{12} = \nu_{12}Q_{22}$ is constant (independent of S) yields a damage evolution ordinary differential equation which can be solved for S.

$$\frac{\epsilon_{22}^2}{2}\frac{\partial E_{22}}{\partial S} + \frac{\gamma_{12}^2}{2}\frac{\partial G_{12}}{\partial S} = -1 \tag{11}$$

The above equation indicates that the work of structural change depends only on the strain state,the initial virgin composite moduli, E_{220} and G_{120}, and the damage functions, $e_s(S)$ and $g_s(S)$.

Experimentally, it has been determined that S behaves as ϵ^3, thus it is convenient to introduce a reduced damage variable, S_r.[18]

$$S_r \equiv S^{1/3} \tag{12}$$

Furthermore, the use of a reduced ISV transforms the damage functions into polynomial functions. Using the reduced ISV the evolution equation, Equation (11), becomes

$$\frac{\epsilon_{22}^2}{2}\frac{\partial E_{22}}{\partial S_r} + \frac{\gamma_{12}^2}{2}\frac{\partial G_{12}}{\partial S_r} = -3S_r^2 \tag{13}$$

Once S is determined from Equation (13), the transverse and shear moduli can be degraded accordingly using Equations (8) and (9). Sicking[18] uses this formulation to successfully predict the nonlinear response of numerous coupon laminates.

As a material point is loaded, the fibers begin to rotate. All calculations are performed in the instantaneous material frame by tracking the fiber angle and transforming the field variables accordingly. These rotations induce large, localized shear strains which degrade the matrix shear modulus, offering less resistance to further fiber rotation. If the loading is compressive, this feedback leads to runaway instabilities and regions of microbuckled, or kinked, fibers will develop. Previous studies,[25,43] where the loading was compression dominated, capture the instantaneous fiber rotation in conjunction with ST. This has the advantage of predicting fiber kinking failure, avoiding the use of an explicit fiber direction compressive strength criterion. Moving away from the use of "strength" criteria and instead developing mechanism based failure models is a major objective of the ongoing research.

III. Micromechanical Modeling Using the Generalized Method of Cells: the fiber/matrix scale

A micromechanical analysis technique, coined the Method of Cells, was developed by Aboudi;[62] subsequently, Paley and Aboudi[58] expanded the Method of Cells into the Generalized Method of Cells, and later Aboudi et al.[63] further increased the robustness of this method with the High Fidelity Method of Cells (HFGMC). These methods provide semi-closed form solutions for determining global anisotropic composite properties in terms of the constituent materials, as well as, the fully three dimensional (3-D) stresses and strains in each of the constituent subcells. The sophisticated methods (GMC and HFGMC) offer a high degree of accuracy at a relatively low computational cost. The following sections detail the formulation of GMC (employed herein). The reader is referred to Ref. 63 for details on HFGMC.

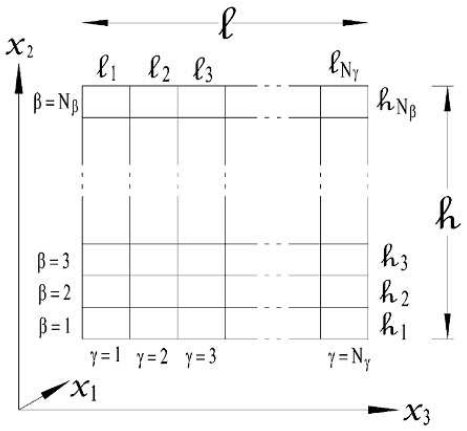

Figure 3. Repeating volume element used in GMC.

III.A. Kinematics and constitutive relationships

It is assumed that a unidirectional fiber composite can be represented as a collection of RVEs. Paley and Aboudi[58] chose to model this RVE as an element consisting of N_β x N_γ $(\beta, \gamma = 1, 2, N_{\beta,\gamma})$ subcells as shown in Figure 3.[58] Each of these subcells are occupied by one of the constituents in the composite. The number of subcells and the materials occupying each subcell are completely general. For a two-phase fibrous composite any desired micro-architecture can be represented by occupying each subcell with either a matrix or fiber constituent. The x_1-axis shown in Figure 3 is the fiber direction, and it is assumed that the RVE extends infinitely in that direction. The cross-sectional area of each subcell is given by $h_\beta \ell_\gamma$. A local coordinate system $(x_1, \bar{x}_2^{(\beta)}, \bar{x}_3^{(\gamma)})$ can be introduced with its origin located at the center of each subcell, as shown in Figure 4.[58]

The objective of this method is to determine the average behavior of the composite material; thus, it is sufficient to model the displacements in each subcell using a linear theory (HFGMC employs a higher order displacement approximation).

$$u_i^{(\beta\gamma)} = w_i^{(\beta\gamma)} + \bar{x}_2^{(\beta)} \phi_i^{(\beta\gamma)} + \bar{x}_3^{(\gamma)} \psi_i^{(\beta\gamma)} \tag{14}$$

where $i = 1, 2, 3$, $w_i^{(\beta\gamma)}$ is the displacement at the center of subcell $\beta\gamma$. Microvariables $(\phi_i^{(\beta\gamma)}, \psi_i^{(\beta\gamma)})$ characterize the first-order dependence of the displacement field on the local coordinates $\bar{x}_2^{(\beta)}$ and $\bar{x}_3^{(\gamma)}$.

The components of the strain tensor follow from Equation (14) as,

$$\epsilon_{ij}^{(\beta\gamma)} = \frac{1}{2}\left(\partial_i u_j^{(\beta\gamma)} + \partial_j u_i^{(\beta\gamma)}\right) \tag{15}$$

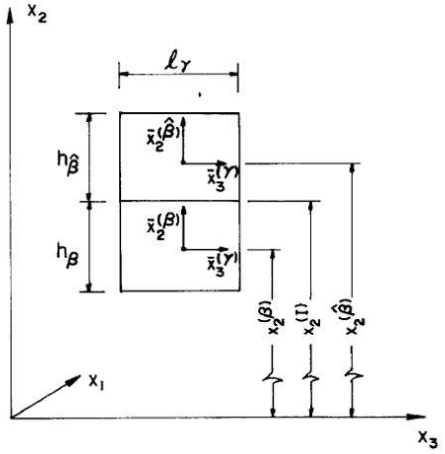

Figure 4. Local coordinates used in GMC subcells.

where $\partial_1 = \frac{\partial}{\partial x_1}, \partial_2 = \frac{\partial}{\partial \bar{x}_2^{(\beta)}}, \partial_3 = \frac{\partial}{\partial \bar{x}_3^{(\gamma)}}$. Substituting Equation (14) into Equation (15) results in the six components of the average strain tensor for each subcell in terms of the microvariables.

$$\begin{aligned}
\bar{\epsilon}_{11}^{(\beta\gamma)} &= \partial_1 w_1^{(\beta\gamma)} \\
\bar{\epsilon}_{22}^{(\beta\gamma)} &= \phi_2^{(\beta\gamma)} \\
\bar{\epsilon}_{33}^{(\beta\gamma)} &= \psi_3^{(\beta\gamma)} \\
2\bar{\epsilon}_{23}^{(\beta\gamma)} &= \phi_3^{(\beta\gamma)} + \psi_2^{(\beta\gamma)} \\
2\bar{\epsilon}_{13}^{(\beta\gamma)} &= \psi_1^{(\beta\gamma)} + \partial_1 w_3^{(\beta\gamma)} \\
2\bar{\epsilon}_{12}^{(\beta\gamma)} &= \phi_1^{(\beta\gamma)} + \partial_1 w_2^{(\beta\gamma)}
\end{aligned} \tag{16}$$

The constitutive law also needs to be defined for each subcell, and can use any stress-strain relationship desired. In this work, it will be assumed that only elastic subcell strains, $\bar{\epsilon}_{ij}^{(\beta\gamma)}$, are present. However, the constitutive law can be amended to incorporate additional strains such as thermal and inelastic strains. Hooke's law for relating the stresses to the elastic strains can be written as

$$\bar{\sigma}_{ij}^{(\beta\gamma)} = C_{ijkl}^{(\beta\gamma)} \bar{\epsilon}_{kl}^{(\beta\gamma)} \tag{17}$$

where $C_{ijkl}^{(\beta\gamma)}$ are the components of the elastic stiffness tensor.

III.B. Displacement continuity conditions

It is required that subcell displacements are continuous at the interfaces between adjacent subcells, as well as at the boundaries between neighboring repeating cells. Enforcing these conditions will yield $2(N_\beta + N_\gamma) + N_\beta N_\gamma + 1$ equations. Moreover all microvariables are eliminated from these equations by casting the displacement continuity conditions in terms of the average strains. For detailed derivations of displacement and traction continuity conditions see Ref. 58.

The first necessary equation is obtained by defining the average strains (obtained from homogenous boundary conditions) in the composite, $\bar{\epsilon}_{ij}$, in terms of the average subcell strains.

$$\bar{\epsilon}_{ij} = \frac{1}{h\ell} \sum_{\beta=1}^{N_\beta} \sum_{\gamma=1}^{N_\gamma} h_\beta \ell_\gamma \bar{\epsilon}_{ij}^{(\beta\gamma)} \tag{18}$$

where h, ℓ and h_β, ℓ_γ represent the RVE, and subcell geometry, respectively (see Figures 3 and 4).

The linear displacement fields yield uniform, or average, strain fields in each subcell. Therefore, displacement continuity is satisfied in an average sense over all subcell and repeating cell interfaces using the strains. Since these continuity conditions are satisfied on average, the shape of the subcells does not appear in the final result. Thus, no stress concentrations are developed at the corners, and the end result is that the subcell strains, and stresses, are determined as a function of only the fiber volume fraction and constituent properties.

After enforcing average displacement continuity on the interfaces, the following $2(N_\beta + N_\gamma)$ equations are pro-

duced:

$$\sum_{\beta=1}^{N_\beta} h_\beta \bar{\epsilon}_{22}^{(\beta\gamma)} = h\bar{\epsilon}_{22}, \qquad \gamma = 1, \ldots, N_\gamma \tag{19}$$

$$\sum_{\gamma=1}^{N_\gamma} \ell_\gamma \bar{\epsilon}_{33}^{(\beta\gamma)} = \ell\bar{\epsilon}_{33}, \qquad \beta = 1, \ldots, N_\beta \tag{20}$$

$$\sum_{\beta=1}^{N_\beta} h_\beta \bar{\epsilon}_{12}^{(\beta\gamma)} = h\bar{\epsilon}_{12}, \qquad \gamma = 1, \ldots, N_\gamma \tag{21}$$

$$\sum_{\gamma=1}^{N_\gamma} \ell_\gamma \bar{\epsilon}_{13}^{(\beta\gamma)} = \ell\bar{\epsilon}_{13}, \qquad \beta = 1, \ldots, N_\beta \tag{22}$$

An additional $N_\beta N_\gamma$ equations result from enforcing uniform strain in the x_1-direction across all subcells.

$$\bar{\epsilon}_{11}^{(\beta\gamma)} = \bar{\epsilon}_{11} \tag{23}$$

The final equation is obtained by evaluating Equation (18) with $i = 2$ and $j = 3$.

$$\bar{\epsilon}_{23} = \frac{1}{h\ell} \sum_{\beta=1}^{N_\beta} \sum_{\gamma=1}^{N_\gamma} h_\beta \ell_\gamma \bar{\epsilon}_{23}^{(\beta\gamma)} \tag{24}$$

Equations (19) - (24) can be rearranged and rewritten in matrix from.

$$\mathbf{A}_G \epsilon_S = \mathbf{J}\bar{\epsilon} \tag{25}$$

where

$$\bar{\epsilon} = \{\bar{\epsilon}_{11}, \bar{\epsilon}_{22}, \bar{\epsilon}_{33}, 2\bar{\epsilon}_{23}, 2\bar{\epsilon}_{13}, 2\bar{\epsilon}_{12}\} \tag{26}$$

and

$$\epsilon_S = \left[\bar{\epsilon}^{(11)}, \bar{\epsilon}^{(12)}, \ldots, \bar{\epsilon}^{(N_\beta N_\gamma)}\right] \tag{27}$$

where $\bar{\epsilon}^{(\beta\gamma)}$ are vectors containing the average subcell strains in the same order as Equation (26).

III.C. Traction continuity conditions

Traction continuity must also be enforced in order to arrive at the correct number of equations needed to solve for the $6N_\beta N_\gamma$ subcell strain unknowns. However, some of the traction continuity conditions are redundant. After eliminating repeating traction continuity conditions, the following $5N_\beta N_\gamma - 2(N_\beta + N_\gamma) - 1$ independent equations remain:

$$\bar{\sigma}_{22}^{(\beta\gamma)} = \bar{\sigma}_{22}^{(\hat{\beta}\gamma)}, \quad \beta = 1, \ldots, N_\beta - 1, \quad \gamma = 1, \ldots, N_\gamma \tag{28}$$

$$\bar{\sigma}_{33}^{(\beta\gamma)} = \bar{\sigma}_{33}^{(\beta\hat{\gamma})}, \quad \beta = 1, \ldots, N_\beta, \quad \gamma = 1, \ldots, N_\gamma - 1 \tag{29}$$

$$\bar{\sigma}_{23}^{(\beta\gamma)} = \bar{\sigma}_{23}^{(\hat{\beta}\gamma)}, \quad \beta = 1, \ldots, N_\beta - 1, \quad \gamma = 1, \ldots, N_\gamma \tag{30}$$

$$\bar{\sigma}_{32}^{(\beta\gamma)} = \bar{\sigma}_{32}^{(\beta\hat{\gamma})}, \quad \beta = 1, \ldots, N_\beta, \quad \gamma = 1, \ldots, N_\gamma - 1 \tag{31}$$

$$\bar{\sigma}_{21}^{(\beta\gamma)} = \bar{\sigma}_{21}^{(\hat{\beta}\gamma)}, \quad \beta = 1, \ldots, N_\beta - 1, \quad \gamma = 1, \ldots, N_\gamma \tag{32}$$

$$\bar{\sigma}_{31}^{(\beta\gamma)} = \bar{\sigma}_{31}^{(\beta\hat{\gamma})}, \quad \beta = 1, \ldots, N_\beta, \quad \gamma = 1, \ldots, N_\gamma - 1 \tag{33}$$

where $\hat{\beta}$ and $\hat{\gamma}$ are given by

$$\hat{\beta} = \begin{cases} \beta + 1, & \beta < N_\beta \\ 1, & \beta = N_\beta \end{cases} \tag{34}$$

$$\hat{\gamma} = \begin{cases} \gamma + 1, & \gamma < N_\gamma \\ 1, & \gamma = N_\gamma \end{cases} \tag{35}$$

These traction conditions can be recast in terms of the average subcell strains using the constitutive relationship, in this case Equation (17). The equations can then be rewritten in matrix form.

$$\mathbf{A}_M \epsilon_S = \mathbf{0} \tag{36}$$

where ϵ_S is given in Equation (27)

III.D. Determining subcell strains

Once $\mathbf{A}_G$, $\mathbf{A}_M$, and $\mathbf{J}$ have been determined, the subcell strains can be computed by solving

$$\tilde{\mathbf{A}} \epsilon_S = \mathbf{K} \bar{\epsilon} \tag{37}$$

where

$$\tilde{\mathbf{A}} = \begin{bmatrix} \mathbf{A}_M \\ \mathbf{A}_G \end{bmatrix} \tag{38}$$

and

$$\mathbf{K} = \begin{bmatrix} \mathbf{0} \\ \mathbf{J} \end{bmatrix} \tag{39}$$

After the subcell strains are obtained, it is trivial to produce the subcell stresses using the constitutive law.

III.E. Micro-constituent failure

The multiscale computational method employed in the FEM simulations uses GMC to resolve the applied global stresses to the micro-constituent level. Failure of the matrix phase, meant to represent failure due to transverse cracking, is established using the 3-D Tsai-Hill failure criterion.[9] Assuming failure in the matrix subcells is isotropic, the criterion is given as

$$\begin{aligned} &\frac{\left(\bar{\sigma}_{11}^{(\beta_m\gamma_m)}\right)^2 + \left(\bar{\sigma}_{22}^{(\beta_m\gamma_m)}\right)^2 + \left(\bar{\sigma}_{33}^{(\beta_m\gamma_m)}\right)^2}{Y_{mt}^2} \\ &+ \frac{-\bar{\sigma}_{11}^{(\beta_m\gamma_m)}\bar{\sigma}_{22}^{(\beta_m\gamma_m)} - \bar{\sigma}_{11}^{(\beta_m\gamma_m)}\bar{\sigma}_{33}^{(\beta_m\gamma_m)} - \bar{\sigma}_{22}^{(\beta_m\gamma_m)}\bar{\sigma}_{33}^{(\beta_m\gamma_m)}}{Y_{mt}^2} \\ &+ \frac{\left(\bar{\sigma}_{12}^{(\beta_m\gamma_m)}\right)^2 + \left(\bar{\sigma}_{13}^{(\beta_m\gamma_m)}\right)^2 + \left(\bar{\sigma}_{23}^{(\beta_m\gamma_m)}\right)^2}{T_m^2} = d_m^2, \quad \bar{\sigma}_{22} > 0 \end{aligned} \tag{40}$$

where β_m and γ_m are the matrix subcell indices and the average applied transverse stress, $\bar{\sigma}_{22}$, is tensile. Similarly, for applied compressive transverse stresses:

$$\begin{aligned} &\frac{\left(\bar{\sigma}_{11}^{(\beta_m\gamma_m)}\right)^2 + \left(\bar{\sigma}_{22}^{(\beta_m\gamma_m)}\right)^2 + \left(\bar{\sigma}_{33}^{(\beta_m\gamma_m)}\right)^2}{Y_{mc}^2} \\ &+ \frac{-\bar{\sigma}_{11}^{(\beta_m\gamma_m)}\bar{\sigma}_{22}^{(\beta_m\gamma_m)} - \bar{\sigma}_{11}^{(\beta_m\gamma_m)}\bar{\sigma}_{33}^{(\beta_m\gamma_m)} - \bar{\sigma}_{22}^{(\beta_m\gamma_m)}\bar{\sigma}_{33}^{(\beta_m\gamma_m)}}{Y_{mc}^2} \\ &+ \frac{\left(\bar{\sigma}_{12}^{(\beta_m\gamma_m)}\right)^2 + \left(\bar{\sigma}_{13}^{(\beta_m\gamma_m)}\right)^2 + \left(\bar{\sigma}_{23}^{(\beta_m\gamma_m)}\right)^2}{T_m^2} = d_m^2, \quad \bar{\sigma}_{22} < 0 \end{aligned} \tag{41}$$

where Y_{mt} and Y_{mc} are the matrix transverse tensile and compressive strengths, respectively, and T_m is the matrix shear strength.

A maximum strain criterion is used to dictate tensile failure in the fiber subcells.

$$\left(\frac{\bar{\epsilon}_{11}^{(\beta_f \gamma_f)}}{\epsilon_{ft}^{U}}\right)^2 = d_f^2, \quad \bar{\epsilon}_{11} > 0 \tag{42}$$

where β_f and γ_f are the fiber subcell indices, ϵ_{ft}^{U} is the tensile ultimate fiber strain, and $\bar{\epsilon}_{11}$ is the applied axial strain. Fiber failure in compression is accounted for automatically at the lamina level through fiber rotation (see Section II.C.

Failure arises in matrix subcells when $d_m \geq 0$ and in fiber subcells when $d_f \geq 0$ for that subcell. Once a subcell has failed, all the properties of that subcell are degraded appropriately.

IV. Multiscale Model

A multiscale coupled microdamage-failure finite element model was developed using the commercially available ABAQUS[54] FE package and the MAC/GMC Suite of Micromechanics Codes,[55,56] developed at the NASA Glenn Research Center. This model is used to simulate the behavior of a notched carbon fiber reinforced epoxy panel from Ref. 60, shown in Figure 5.[60] Two laminate stacking sequences, shown in Table 1, are modeled, and the elastic properties corresponding to T800/3900-2 (Table 2) are used as the initial properties for each layer.

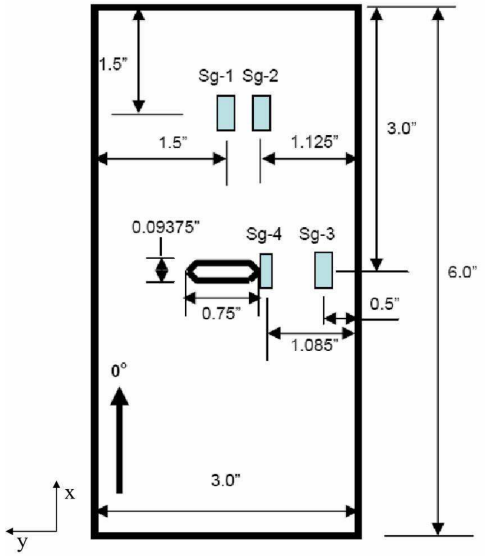

Figure 5. Experimental diagram displaying locations of strain gages on notched specimens used to validate FE model results.

ID	Stacking Sequence	Thickness (in.)
Laminate Sequence-1	$[0]_{12}$	0.078
Laminate Sequence-2	$[45/0/\text{-}45/0/90]_S$	0.065

Table 1. Laminate stacking sequences investigated.

Property	Value
E_{11} (Msi)	23.2
E_{22} (Msi)	1.3
G_{12} (Msi)	0.9
ν_{12}	0.28

Table 2. Initial elastic properties of T800/3900-2 lamina.

The mesh used in the FEM model, shown in Figure 6, consists of 8864 nodes and 9821 ABAQUS S4R quadrilateral and S3R triangular elements. A mesh density of 10 elements within one notch radius is used near the notch (Figure

6(b)), which is necessary to produce reasonably accurate stress and strain fields and gradients in the presence of a cut-out.[64] No constraints were placed on the vertical edges of the model, and the bottom edge was restricted from moving in the x, y, z, and all rotational degrees of freedom. The top edge is fixed in the y, and z displacements and all rotations. A vertical displacement is applied in the x direction to simulate tensile loading.

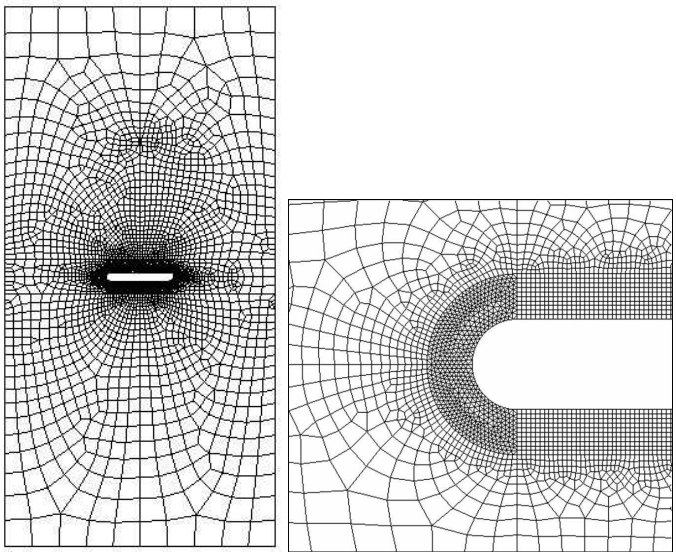

(a) FEM Mesh used in simulations.

(b) Enlarged view of mesh near notch tip

Figure 6.

Static analysis is performed in both ABAQUS/Standard and ABAQUS/Explicit. An edge displacement of 0.025 in. and 0.065 in. is applied to laminate stacking sequence 1 and 2, respectively. In ABAQUS/Standard the maximum allowable displacement in each time step was set to 0.1%, and the minimum allowed displacement was 0.1E-7%. In ABAQUS/Explicit, the total displacement was applied over 0.01 seconds using the ABAQUS amplitude definition *AMPLITUDE, DEFINITION=SMOOTH STEP. A smooth step displacement is chosen to reduce oscillations that arise in the kinetic energy of the system when using linear displacement.[54] A study was conducted on the 0^o laminate that determined that 0.01 seconds is an adequate simulation duration that can be used without any dynamic effects arising. The critical stable time increments calculated by ABAQUS are 1.46E-2 μs for laminate sequence-1, and 1.21E-2 μs for laminate sequence-2. However, to further reduce the computational cost of the explicit model, mass scaling was introduced using the ABAQUS command *FIXED MASS SCALING. The mass of the elements are scaled at the beginning of the step so that the stable time increment is greater than 1 μs. This scaling occurs every 1000 increments using *VARIABLE MASS SCALING.

ST was implemented at the lamina level to model progressive microdamage using the ABAQUS user subroutine UMAT for ABAQUS/Standard and VUMAT for ABAQUS/Explicit. The reduced damage state, S_r, is calculated at each integration point using Equation (13). The damage functions, e_s, and g_s given in Equations (8) and (9) were calibrated using the local strain gage data from laminate sequence-1. Third order polynomial fits of these curves are used, so that the evolution equation, Equation (13), reduces to a quadratic equation for S_r. The polynomials are presented in Figure 7.

At each material point, MAC/GMC is called and a 2 x 2 RVE, shown in Figure 8, is used to model that point. The RVE consists of 3 matrix subcells, shaded green, and 1 fiber subcell, shaded blue. The software FEAMAC,[46] developed by NASA Glenn, is used to communicate between MAC/GMC and the ABAQUS/Standard user subroutine UMAT; whereas FEAMAC/Explicit,[65] recently developed by NASA Glenn and the University of Michigan, couples MAC/GMC to ABAQUS/Explicit using the unchanged FEAMAC UMAT and a VUMAT. The fiber and matrix constituents have the initial properties given in Table 3. To provide global properties consistent with those given in Table 2 anisotropic properties were used for the constituent cells. A square-packing architecture was chosen for this simulation, due to its low computational costs; however any architecture could have been chosen.

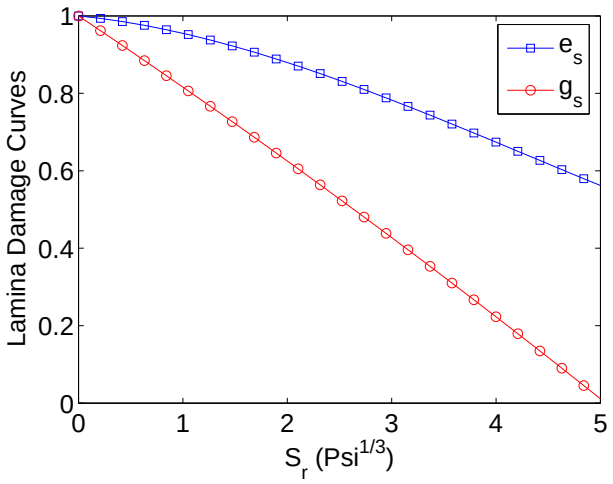

Figure 7. Damage curves used in ST to govern dependence of E_{22} and G_{12} on S_r.

Fiber Properties	Values	Matrix Properties	Values
E_{11}^f (Msi)	42.69	E_{11}^m (Msi)	0.3414
E_{22}^f (Msi)	13.20	E_{22}^m (Msi)	0.3414
ν_{12}^f	0.2316	ν_{12}^m	0.35
ν_{21}^f	0.45	ν_{21}^m	0.35
G_{12}^f (Msi)	8.0	G_{12}^m (Msi)	0.3270

Table 3. Elastic properties of fiber and matrix constituents used in GMC.

At every time step, the micromechanics model must produce composite moduli that are consistent with the lamina level moduli calculated using Equations (8) and (9). Therefore, it is necessary that the moduli of the matrix constituents degrade in a manner that produces consistent E_{22}, and G_{12} values. Two fourth order polynomials are used to calculate the matrix Young's Modulus and shear modulus, E_m and G_m, as a function of S_r, shown in Figure 9. The matrix Poisson's Ratio, ν_m, remains unchanged.

An additional ISV may have been used to model transverse cracking; although, in this preliminary work, failure criteria are evaluated at the micro-level using the subcell stresses calculated by GMC to mark the end of matrix microdamage and the transition to transition to transverse cracking, as well as fiber breakage. Subsequently, the local failure behavior is instantaneous, but the overall effects of subcell failure on a material point are somewhat progressive. Since large portions of the panels experience little to no damage and are unlikely to exhibit failure, the micromechanical failure analysis is only executed at material points where S_r >15 $\text{Pa}^{\frac{1}{3}}$. The constituent failure strengths used are given in Table 4. The matrix constants were calibrated using laminate sequence-1; whereas, the fiber failure constants were calibrated using laminate sequence-2 since laminate sequence-1 exhibited no fiber failure. The properties of any subcell satisfying the failure criterion are reduced by 99.9%. Once failure has occurred in any subcell, progressive damage is deactivated at that integration point. Figure 10 displays a flowchart detailing the entire

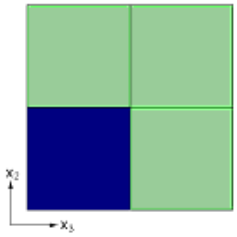

Figure 8. 2 x 2 RVE used in micromechanics simulations.

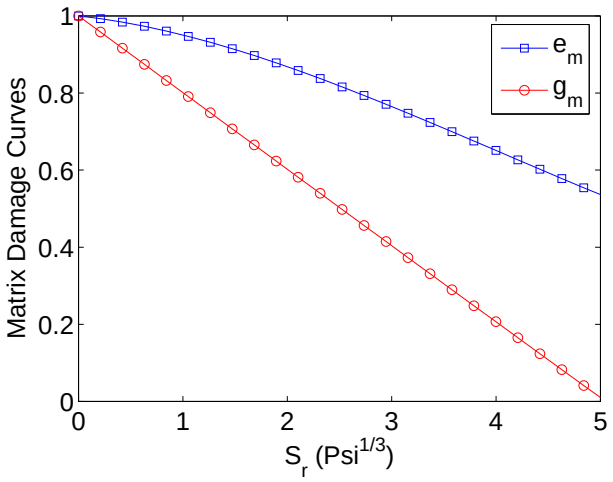

Figure 9. Micro-level damage curves used in MAC/GMC to provide lamina level properties consistent with those calculated by ST for a given S_r.

multiscale algorithm.

Table 4. Constituent failure strengths.

Property	Value
Y_{mt} (msi)	0.0214
Y_{mc} (msi)	0.1751
T_m (msi)	0.0155
ϵ_{ft}^U	0.0435

V. Results and Discussion

Applied load versus edge displacement and applied load versus local strain gage data is compared against experimental results from Ref. 60 in this section. Additionally, predicted damage and failure paths are compared to C-scans and photographs of tested specimens. Results for a third laminate, presented in Ref. 60, have not been included due to a large degree of delamination observed in experiment which was not incorporated into the current model.

V.A. Laminate sequence-1

Load versus edge displacement data for laminate sequence-1 is displayed in Figure 11. The explicit results match very closely with the experimental results. However, the standard results failed to converge at a maximum displacement of 0.0024 in. Due to this, S_r was limited to values less than or equal to 2.89 psi$^{\frac{1}{3}}$. This limit insures that microdamage does not cause any material softening in the transverse or shear response. However once matrix failure onsets, large, sudden changes occur in the shear and transverse properties and the solution diverges at a maximum displacement of 0.01 in.

The applied load versus local strain results provide further information. The non-linear stiffness at sg-1,2, and 3 closely follow the experimental results up to around 8000 lbf. After this point, matrix splitting propagates from the notch tips perpendicular to the notch. This is marked by strain relaxation at sg-1. The explicit method reasonably captures the splitting load; however it subsequently deviates from the experimental data. The standard analysis, with an imposed limit on the maximum value of S_r, does not accurately capture the splitting load, and the solution diverges right after splitting due to failure occurs. Damage and failure contour plots (see Figure 13) reveal that both damage and failure are present at the splitting load. This indicates that failure failure behavior in these analyses are coupled with microdamage. Limiting the damage affected the activation of failure, and thus, requires a different set of failure constants for accurate results. Similar results are observed for sg-2 and 3. There is significant error in the results for sg-4. However, this is somewhat expected. Since sg-4 is directly in front of the notch (a region containing very large

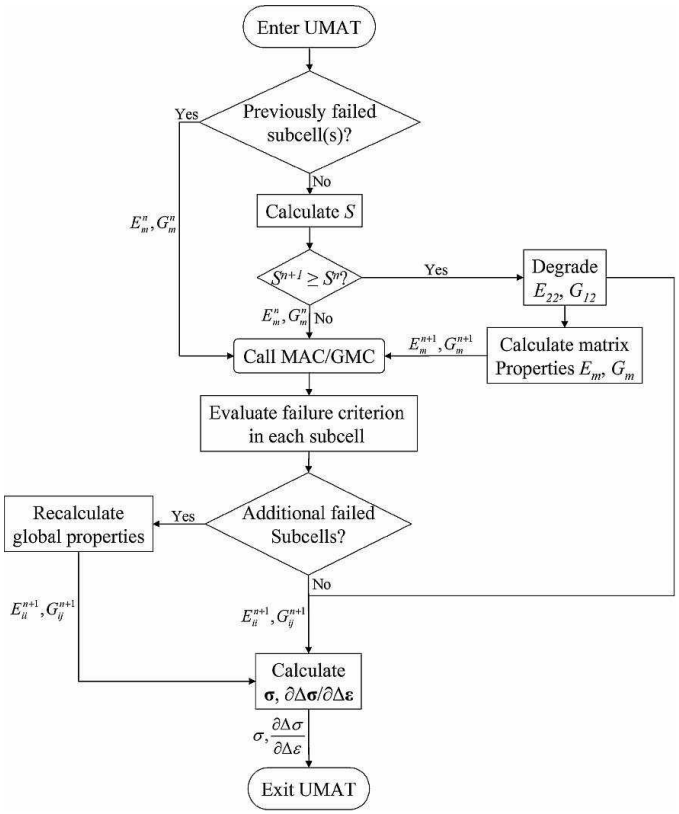

Figure 10. Algorithm used in both explicit and standard simulations. The explicit simulations use the same UMAT, but a VUMAT coordinates between the UMAT and ABAQUS/Explicit.

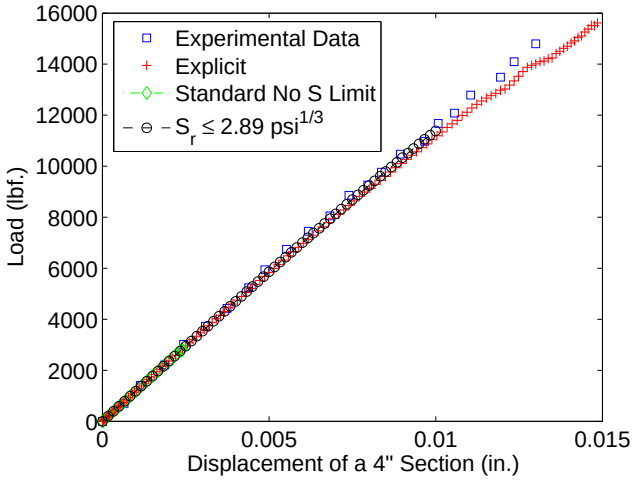

Figure 11. Load versus displacement of a 4" section, laminate sequence-1.

stress and strain gradients) it is imperative to know exactly what points the gage is measuring data from if accurate results are expected. Although, the shape of the load-strain curve at sg-4 is captured with the explicit method.

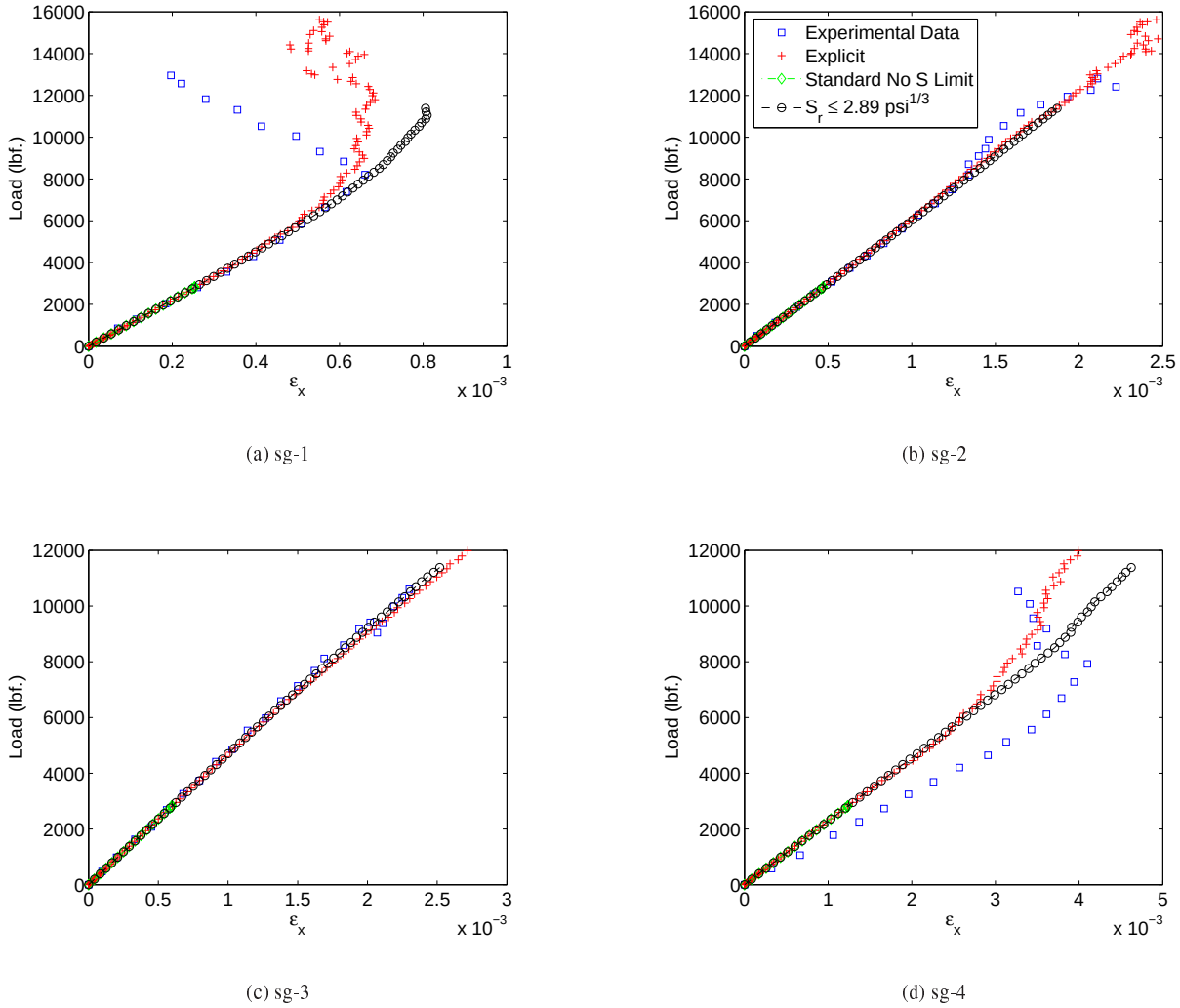

(a) sg-1

(b) sg-2

(c) sg-3

(d) sg-4

Figure 12. Load vs. strain for laminate sequence-1.

The damage and failure patterns produced by the ABAQUS/Explicit simulation are displayed at the splitting load in Figure 13 along with a C-scan of a failed specimen. Both the damage and failure patterns exhibit the splitting behavior present in the C-scan. The colored elements in the failure pattern contour represent the number of failed subcells in the micro-model. Turquoise, yellow, and green indicate one, two, and three failed matrix subcells, respectively; whereas, when all three matrix subcells as well as the fiber subcell have failed, the element is removed from the simulation. The damage contours represent the continuous reduced damage ISV, S_r. Red marks the maximum damage level (S_r=5.50 psi$^{\frac{1}{3}}$). The failed regions in Figure 13(a) match closely with the areas that have reached maximum damage in Figure 13(b). No fiber failure is evident in either the experiment or simulations up to the splitting load.

V.B. Laminate sequence-2

Figure 14 displays the load versus displacement results for the three models and the experiment. The explicit simulation is able to accurately capture the ultimate load measured from the uniaxial tension tests. After fiber failure is initiated, a large amount of energy is transferred to kinetic energy and the specimen fails catastrophically. This may signal that the mass scaling used to increase the stable time step is introducing fictitious inertial effects in this model upon the initiation of fiber failure. Using the same failure constants as the explicit model, the standard simulations with and without imposed limit on S_r diverge at a load greater than the ultimate load. This implies that, initially,

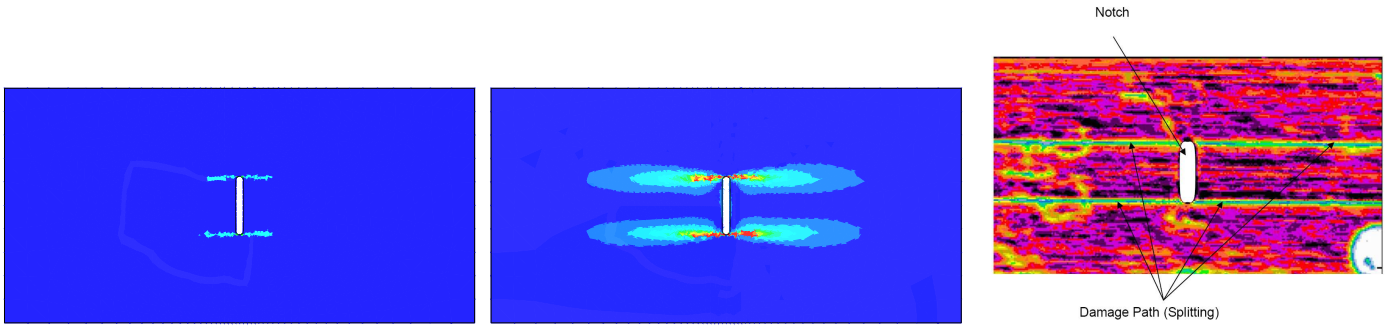

(a) Failure pattern, P=8,983 lbf.

(b) Damage pattern, P = 8,983 lbf.

(c) C-Scan of failed laminate-1 specimen exhibiting splitting.[60]

Figure 13. Failure and damage paths in 0° layer of laminate sequence-1.

fiber failure initiation does not trigger specimen failure in the implicit schemes (standard). However, it is unclear if the standard simulations are diverging at the ultimate load because there is no drop in load subsequent to divergence. Furthermore, the implicit model that left S_r unrestricted converged farther than the limiting case. This suggests that divergence of the simulations of laminate sequence-2 are a result of large, sudden changes in material properties due to failure, not microdamage.

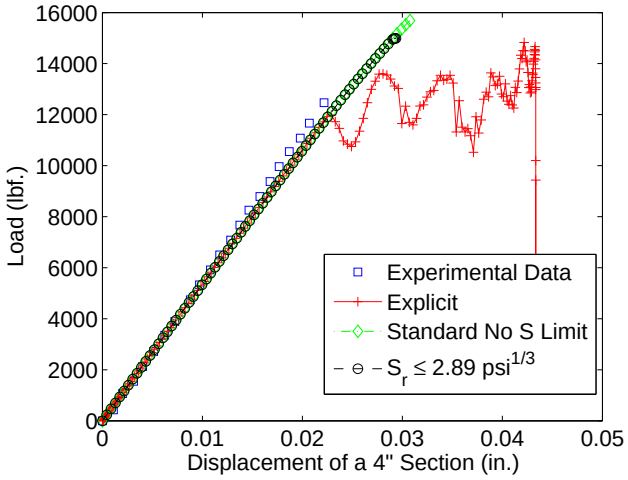

Figure 14. Load versus displacement of a 4" section, laminate sequence-2.

The local strain gage data and predictions are presented in Figure 15. The standard and explicit results are identical up to the onset of specimen failure in the explicit model. The results are very agreeable for sg-1 and sg-2. There is some deviation from experiment in the results for sg-3. The predictions for sg-4 are erroneous; however this is expected due to the high stress and strain gradients near the notch and uncertainty in the experimental strain gage measurements (as was the case for sg-4 on laminate sequence-1).

Figures 16 and 18 display the damage and failure contours in laminate sequence-2 produced by the explicit model at the specimen ultimate load. The same contour color scales that are used for laminate sequence-1 are used for laminate sequence-2. Again, matrix failure is limited to regions of maximum damage. Minimal amounts of matrix failure arise in all layers of the laminate. The 45^o and 90^o layers experience significant damage throughout the entire laminae. The damage in the 0^0 plies are restricted to areas around the notch. Cracks, represented by fiber failure (removed elements), form at the notch tips and propagate, parallel to the notch, towards the free edges. An enlarged view of the notch is given in Figure 17 exhibiting the fiber failure. At the ultimate load for the specimen, the size of the regions containing fiber failure are small relative to the width of the specimen. It can be inferred, that in the explicit case for a center-notch plate, the onset of fiber failure cause catastrophic failure of the panel.

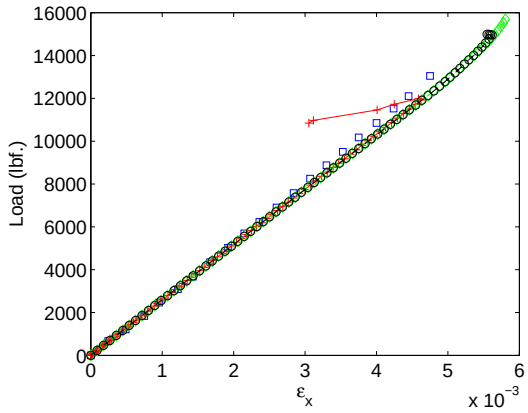

(a) sg-1

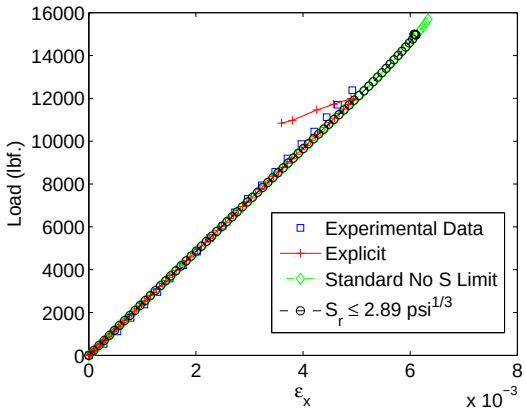

(b) sg-2

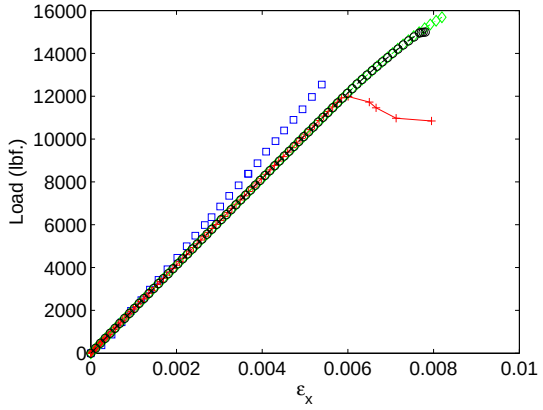

(c) sg-3

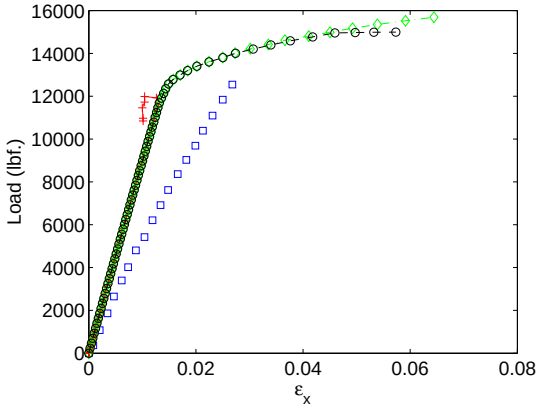

(d) sg-4

Figure 15. Load vs. strain for laminate sequence-2.

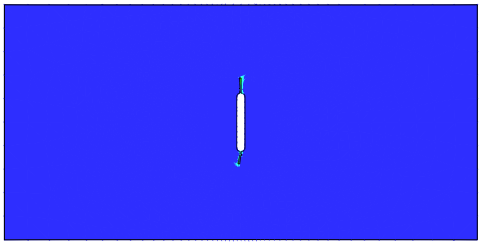

(a) Failure pattern, P=11,990 lbf.

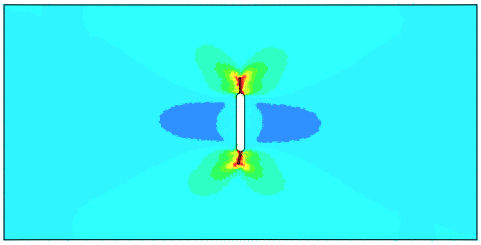

(b) Damage pattern, P = 11,990 lbf.

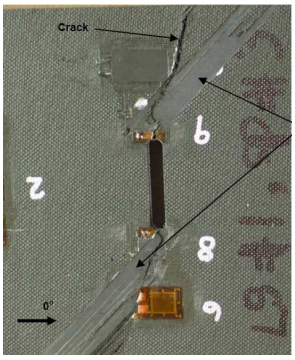

(c) Photograph of failed laminate sequence-2 specimen.[60]

Figure 16. Failure and damage paths in 45° layer of laminate sequence-2.

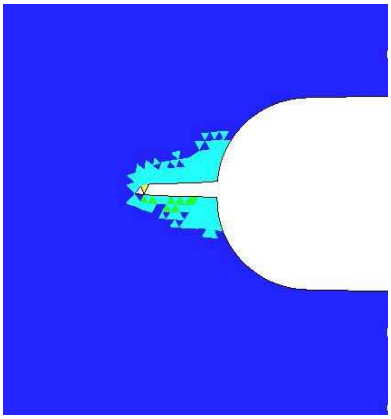

Figure 17. Enlarged view of fiber failure near notch tip in laminate sequence-2.

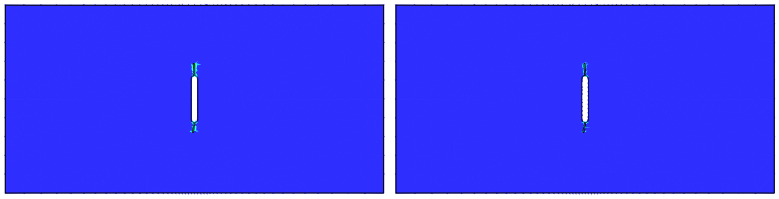

(a) Failure pattern in 0° layer.

(b) Failure pattern in 90° layer.

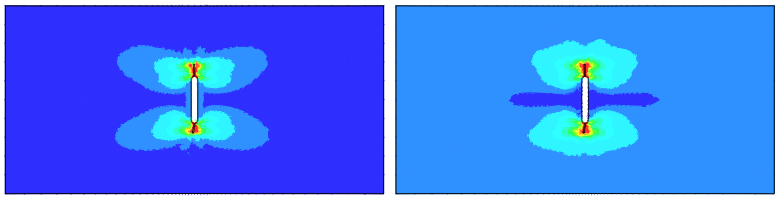

(c) Damage pattern in 0° layer.

(d) Damage pattern in 90° layer.

Figure 18. Failure and damage paths in 0° and 90° layers of laminate sequence-2 at P=11,990 lbf.

VI. Conclusions

A preliminary multiscale model for predicting progressive damage and failure in FRLs was presented. The method models progressive microdamage at the lamina level with ST and uses GMC to model failure due to matrix transverse cracking and fiber breakage by evaluating failure criteria at the micro-constituent level. These models were employed in both implicit and explicit FEM solvers.

The explicit model was able to capture applied load, edge displacement and local strain gage data for two laminates. However, careful attention must be paid to the amount of mass scaling used to increase the critical stable time step and the loading rate so that no undesired dynamic effects arise. To achieve adequate convergence for the $[0^o]$ laminate with ABAQUS/Standard, a limit had to be placed on the maximum level of microdamage. However, restricting the maximum damage level affects the quantitative results. This indicates that the overall behavior of the composite is driven by both mircodamage and failure simultaneously.

Additionally, failure and damage patterns produced by the explicit model are compared. Relatively little failure occurs in the laminates. However, previous studies[51,52,59] using different failure strengths produced significantly more failure. Thus, these simulations are extremely sensitive to the failure constants used.

Future iterations of this model will dispose of failure criteria in favor of more physically based theories to model matrix transverse cracking and fiber failure. Additionally, ST will be implemented directly at the matrix constituent level. Furthermore, failure by delamination will be incorporated into the model. Despite the absence of these features, the current model represents an initial step towards a robust, mechanism-based, multiscale, progressive damage and failure analysis tool for advanced composite structures.

ACKNOWLEDGEMENTS

The authors appreciate the interest and support of Philip Bogert, Alex Tessler, and Arunkumar Satyanarayana at NASA Langely Research Center. This work was supported through a NASA contract to Collier Research Corporation, Collier Subcontract #070327.

References

[1]Beaumont, P. W. R., Dimant, R. A., and Shercliff, H. R., "Failure processes in composite materials: getting physical," *J. Mater. Sci.*, Vol. 41, 2006, pp. 6526–6546.

[2]Hallett, S. R., Jiang, W.-G., Khan, B., and Winsom, M. R., "Modelling the interaction between matrix cracks and delamination damage in scaled quasi-isotropic specimens," *Composites Science and Technology*, Vol. 68, 2008, pp. 80–89.

[3]Pierron, F., Green, B., and Winsom, M. R., "Full-field assessment of the damage process of laminated composite open-hole tensile specimens. Part I: Methodology," *Composites: Part A*, Vol. 38, 2007, pp. 2307–2320.

[4]Pierron, F., Green, B., and Winsom, M. R., "Full-field assessment of the damage process of laminated composite open-hole tensile specimens. Part II: Experimental results," *Composites: Part A*, Vol. 38, 2007, pp. 2321–2332.

[5]Tay, T. E., Liu, G., C., V. B., Tan, Sun, X. S., and Pham, D. C., "Progressive failure analysis of composites," *J. Composite Materials*, Vol. 42, 2008, pp. 1921–1966.

[6]Tsai, S. W., *Strength and Life of Composites*, Aero & Astro, Stanford, 2009.

[7]Hashin, Z. and Rotem, A., "A fatigue failure criterion for fiber reinforced composite materials," *J. Composite Materials*, Vol. 7, 1973, pp. 448–464.

[8]Herakovich, C. T., *Mechanics of Fibrous Composites*, John Wiley & Sons, Inc., 1998.

[9]Jones, R. M., *Mechanics of Composite Materials, 2nd Ed.*, Taylor and Francis, Inc., Philadelphia, 1999.

[10]Soden, P. D., Hinton, M. J., and Kaddour, A. S., "Lamina properties, lay-up configurations and loading conditions for a range of fibre-reinforced composite laminates," *Composites Science and Technology*, Vol. 58, 1998, pp. 1011–1022.

[11]Soden, P. D., Hinton, M. J., and Kaddour, A. S., "A comparison of the predictive capabilites of current failure theories for composite laminates," *Composites Science and Technology*, Vol. 58, 1998, pp. 1225–1254.

[12]Hinton, M. J., Kaddour, A. S., and Soden, P. D., "A comparison of the predictive capabilities of current failure theories for composite laminates, judeged against experimental evidence," *Composites Science and Technology*, Vol. 62, 2002, pp. 1725–1797.

[13]Camanho, P. P., Davila, C. G., Pinho, S. T., Iannucci, L., and Robinson, P., "Prediction of in situ strenghts and matrix cracking in composites under transverse tension and in-plane shear," *Composites: Part A*, Vol. 37, 2006, pp. 165–176.

[14]Daniel, I. M. and Ishai, O., *Engineering Mechanics of Composite Materials, 2nd Ed.*, Oxford University Press, New York, Oxford, 2006.

[15]Talreja, R., "Transverse cracking and stiffness reduction in composite laminates," *J. Composite Materials*, Vol. 19, 1985, pp. 355–275.

[16]Nuismer, R. J. and Tan, S. C., "Constitutive relations of a cracked composite lamina," *J. Composite Materials*, Vol. 22, 1988, pp. 306–321.

[17]Schapery, R. A., "A theory of mechanical behaviour of elastic media with growing damage and other changes in structure," *J. Mech. Phys. Solids*, Vol. 38, No. 2, 1990, pp. 1725–1797.

[18]Sicking, D. L., *Mechanical Characterization of Nonlinear Laminated Composites with Transverse Crack Growth*, Ph.D. thesis, Texas A&M University, College Station, TX, 1992.

[19]Lemaitre, J. and Chaboche, J.-L., *Mechanics of Solid Materials*, Cambridge University Press, 1994.

[20]Ladeveze, P., "Inelastic strains and damage," *Damage Mechanics of Composite Materials*, edited by R. Talreja, Elsevier Science B.V., 1994.

[21]Nairn, J. A. and Hu, S. U., "Matrix microcracking," *Damage Mechanics of Composite Materials*, edited by R. Talreja, Elsevier Science B.V., 1994.

[22]Talreja, R., "Matrix microcracking," *Damage characterization by internal variables*, edited by R. Talreja, Elsevier Science B.V., 1994.

[23]Lemaitre, J., *A Course on Damage Mechanics, 2nd Ed.*, Springer-Verlag, Berlin, Heidelberg, New York, 1996.

[24]McCartney, L. N., "Physically based damage models for laminated composites," *Proc. Instn Mech. Engrs*, Vol. 217, IMechE, 2003, pp. 163–199.

[25]Basu, S., Waas, A. M., and Ambur, D. R., "Compressive failure of fiber composites under multiaxial loading," *Int. J. Solids Structures*, Vol. 44, No. 9, 2006, pp. 2648–2676.

[26]Maimi, P., Camanho, P. P., Mayugo, J. A., and Davila, C. G., "A continuum damage model for composite laminates: Part I - Constitutive model," *Mechanics of Materials*, Vol. 39, 2007, pp. 897–908.

[27]Schuecker, C. and Pettermann, H. E., "Fiber reinforced laminates: progressive damage modeling based on failure mechanisms," *Arch. Comput. Methods Eng.*, Vol. 15, 2008, pp. 163–184.

[28]Sih, G. C. and Chen, E. P., "Fracture analysis of unidirectional composites," *J. Composite Materials*, Vol. 7, 1973, pp. 230–244.

[29]McCartney, L. N., "Mechanics of marix cracking in brittle-matrix fiber-reinforced composites," *Proceedings of the Royal Society of London. Series A, Mathematical and Physical Sciences*, Vol. 409, 1987, pp. 329–350.

[30]Laws, N. and Dvorak, G. J., "Progressive transverse cracking in composite laminates," *J. Composite Materials*, Vol. 22, 1988, pp. 900–916.

[31]McCartney, L. N., "Mechanics for the growth of bridged cracks in composite materials: Part I. Basic Principles," *J. Composites Technology & Research*, Vol. 14, No. 3, 1992, pp. 133–154.

[32]Garikipati, K., *On Strong Discontinuities in Inelastic Solids and their Numerical Simulation*, Ph.D. thesis, Stanford University, Palo Alto, CA, 1996.

[33]Prat, P. C. and Bazant, Z. P., "Tangential stiffness of elastic materials with systems of growing or closing cracks," *J. Mech. Phys. Solids*, Vol. 45, No. 4, 1997, pp. 611–636.

[34]Li, S., Thouless, M. D., Waas, A. M., Schroederd, J. A., and Zavattierid, P. D., "Use of a cohesive zone model to analyze the frcture of a fber-reinfoced polymermatrix composite," *Composites Science and Technology*, Vol. 65, 2005, pp. 537–549.

[35]Yang, Q. and Cox, B., "Cohesive models for damage evolution in laminated composites," *Int. J. Frac.*, Vol. 133, 2005, pp. 107–137.

[36]Xie, D. and Waas, A. M., "Discrete cohesive zone model for mixed-mode fracture using finite element analysis," *Engineering Fracture Mechanics*, Vol. 73, No. 13, 2006, pp. 1783–1796.

[37]Rudraraju, S. S., Vignes, R., Salvi, A., Garikipati, K., and Waas, A. M., "A multiscale crack path predicting computational method for laminated fiber reinforced composites," *49th AIAA/ASME/ASCE/AHS/ASC Structrues, Sturctural Dynamics, and Materials Conference*, 7-10, April 2008.

[38]Budiansky, B. and Fleck, N. A., "Compressive failure of fiber composites," *J. Mech. Phys. Solids*, Vol. 41, No. 1, 1993, pp. 183–211.

[39]Fleck, N. A., Deng, L., and Budiansky, B., "Prediction of kink width in compressed fiber composites," *J. App. Mech.*, Vol. 62, 1995, pp. 329–337.

[40]Schapery, R. A., "Prediction of compressive strength and kink bands in composites using a work potential," *Int. J. Solids Structures*, Vol. 32, No. 6, 1995, pp. 739–765.

[41]Lissenden, C. J. and Arnold, S. M., "Flow/damage surfaces for fiber reinforced metals having different periodic microstructures," *Int. J. Plasticity*, Vol. 16, 2000, pp. 1049–1074.

[42]Yerramalli, C. S. and Waas, A. M., "A failure criterion for fiber reinforced polymer composites under combined compression-torsion loading," *Int. J. Solids Structures*, Vol. 40, No. 5, 2003, pp. 1139–1164.

[43]Basu, S., *Computational Modeling of Progrssive Failure and Damage in Composite Laminates*, Ph.D. thesis, University of Michigan, Ann Arbor, MI, 2005.

[44]Totry, E., Gonzalez, C., and Llorca, J., "Influence of the loading path on the strength of fiber-reinforced composites subjected to transverse compression and shear," *Int. J. Solids Structures*, Vol. 45, 2008, pp. 1663–1675.

[45]Bednarcyk, B. A. and Arnold, S. M., "Full couple micro/macro deformation, damage, and failure prediction for SiC/Ti-15-3 laminates," *J. Aerosp. Eng.*, Vol. 15, No. 3, 2002, pp. 74–83.

[46]Bednarcyk, B. A. and Arnold, S. M., "A framework for performing multiscale stochastic progressive failure analysis of composite structures," *Proceedings of the 2006 ABAQUS User's Conference*, 23-25, May 2006.

[47]Talreja, R., "Multi-scale modeling in damage mechanics of composite materials," *J. Mater. Sci.*, Vol. 41, 2006, pp. 6800–6812.

[48]Belytschko, T., Loehnert, S., and Song, J.-H., "Multiscale aggregating discontinuities: A method for circumventing loss of material stability," *Int. J. Numer. Meth. Engng.*, Vol. 73, 2008, pp. 869–894.

[49]Talreja, R., "Multi-scale modeling of composite solids with damage," *Proceedings of the American Society for Composites Twenty-third Technical Conference*, 9-11, Sept. 2008.

[50]Lee, S., Sundararaghavan, V., and Waas, A., "Multiscale modeling of thermo-mechanical behavior of C-SiC composites," *ASME IMECE Symposium on Advances in Aerospace Technology*, 31 Oct - 8 Nov 2008.

[51]Pineda, E. J., Waas, A. M., Bednarcyk, B. A., Collier, C. S., and Yarrington, P. W., "A novel multiscale physics based progressive failure methodology for laminated composite structures," *49th AIAA/ASME/ASCE/AHS/ASC Structures, Structural Dynamics, and Materials Conference*, 7-10, Apr. 2008.

[52]Pineda, E. J., Waas, A. M., Bednarcyk, B. A., Collier, C. S., and Yarrington, P. W., "A novel multiscale physics based progrssive failure methodology for laminated composite structures," Nasa tm-2008-215448, 2008.

[53]Collier Research Corp., Newport News, VA, *Hypersizer Structural Sizing Software User's Manual*, 2008.

[54]SIMULIA, Providence, RI, *ABAQUS User's Manual, Vol. 1-3, Version 6.7*, 2007.

[55]Bednarcyk, B. A. and Arnold, S. M., "MAC/GMC 4.0 User's Manual - Keywords Manual," Nasa tm-2002-212077/vol2, 2002.

[56]Bednarcyk, B. A. and Arnold, S. M., "MAC/GMC 4.0 User's Manual - Example Problems Manual," Nasa tm-2002-212077/vol3, 2002.

[57]Schapery, R. A. and Sicking, D. L., "A theory of mechanical behaviour of elastic media with growing damage and other changes in structure," *Mechanical Behaviour of Materials*, edited by A. Bakker, Delft University Press, Delft, The Netherlands, 1995, pp. 45–76.

[58]Paley, M. and Aboudi, J., "Micromechanical analysis of composites by the generalized cells model," *Mechanics of Materials*, Vol. 14, 1992, pp. 127–139.

[59]Pineda, E. J., Waas, A. M., Bednarcyk, B. A., and Collier, C. S., "A novel, multiscale high fidelity progressive damage and failure modeling approach for laminated fiber reinforced composites," *Proceedings of the American Society for Composites Twenty-third Technical Conference*, 7-10, Apr. 2008.

[60]Bogert, P. B., Satyanarayana, A., and Chunchu, P. B., "Comparison of damage path predicions for composite laminates by explicit and standard finite element analysis tool," 47^{th} *AIAA Structures, Structural Dynamics, and Materials Conference*, 1-4 May 2006.

[61]Rice, J. R., "Inelastic constitutive relations for solids: an internal-variable theory and its application to metal plasticity," *J. Mech. Phys. Solids*, Vol. 19, 1971, pp. 433–455.

[62]Aboudi, J., *Mechanics of Composite Materials: A Unified Micromechanical Approach*, Elsevier Amsterdam, 1991.

[63]Aboudi, J., Pindera, M.-J., and Arnold, S. M., "Higher-order theory for functionally graded materials," *Composites Part B - Engineering*, Vol. 30, 1999, pp. 777–832.

[64]Bhargava, A. and Shivakumar, K. N., "Three dimensional tensile stress concentration in countersunk rivet holes," *Aeronautical Journal*, Vol. 111, 2007, pp. 777–786.

[65]Pineda, E. J., Waas, A. M., Bednarcyk, B. A., Arnold, S. M., and Collier, C. S., "Multiscale Failure Analysis of Laminated Composite Panels Subjected to Blast Loading Using FEAMAC/Explicit," Nasa tm, submitted April, 2009.